Optimal control of a biomechanical multibody model for the dynamic simulation of working tasks

Michael Roller[1], Staffan Björkenstam [2], Joachim Linn[1], Sigrid Leyendecker[3]

[1]Fraunhofer Institute for Industrial Mathematics
Fraunhofer Platz 1, 67633 Kaiserslautern, Germany
[michael.roller, joachim.linn]@itwm.fraunhofer.de

[2] Fraunhofer-Chalmers Centre
Chalmers Science Park, SE-412 88 Gothenburg, Sweden
staffan.bjorkenstam@fcc.chalmers.se

[3]Chair of Applied Dynamics
University of Erlangen-Nuremberg
Immerwahrstrasse 1, 91058 Erlangen, Germany
sigrid.leyendecker@fau.de

Abstract

In this contribution a framework for digital human modelling using optimal control of a biomechanical multibody model is presented. The skeleton of the human body is represented as a multibody system, actuated by simplified Hill muscles. Motions of the digital human model are generated by optimal control with different objective functions. The optimal control problem is discretized by the DMOCC approach, using a variational integrator for the constrained equations of motion. With this approach, the task of *"lifting of a box from a lower to a higher position"* is simulated as a test example. Both arms are modeled with seven degrees of freedom each, actuated by 29 muscles. In the optimal control problem an arbitrary grasp position is included, as well as frictional contact between the box and the hand.

Keywords: optimal control, biomechanical MBS, hill muscle, assembly simulation

1. Introduction

In industry there is an increasing demand on simulating the dynamic motion of a worker and its interaction with the environment for an ergonomic assessment of tasks, for example the assembly of parts, or moving heavy objects. For given work instructions like *"... move the part from A to B ..."*, a simulation should produce human like motion with realistic joint torques and muscle forces. Optimal control of a biomechanical multibody system [1, 3] is a good approach to create a simulation procedure for a digital human model that fulfills these requirements.

The human skeleton (or parts of it) are modeled as a multibody system (MBS), where, in contrast to [1, 3], a representation with minimal coordinates based on [4] is used due to performance issues [5, 6]. For a MBS with tree-like structure the equations of motion are a system of ordinary differential equation (ODE), turning into a system of differential algebraic equation (DAE) in the case of closed loop kinematics. Realistic inner forces can be obtained by including muscle models into the biomechanical MBS of the digital human. There are a variety of different muscle models [7] with different complexities. As in [3], we restrict ourselves to a string type Hill-model, where the active contractile element (CC) creates a pulling force depending on the actuation, the length and the contraction velocity of the muscle. This CC is connected in parallel to a (non-)linear spring (PEC) that represents the passive stiffness of the tissue. A muscle is attached to the skeletal MBS in at least two body points, connected via a straight line. Hence, if the position and velocity of the bones are known, also the length and the contractile velocity of the muscle can be evaluated. With the help of these quantities and the activation the force F^m can be computed, which is acting on each point of the bones in the direction of the muscle.

Human like motions of such a biomechanical MBS are generated by optimal control, where the control signals are the activations of the muscles. This results in a time continuous optimization problem, including a mathematical model of the working task in the constraints, besides the equations of motion. Motion trajectories with given characteristics like e.g. minimal control effort, minimal kinetic energy or minimal execution time can be generated by choosing a specifically constructed objective. The continuous optimal control problem is solved by applying the so called DMOCC *(discrete mechanics and optimal control for constrained systems)* approach, including a variational integrator to solve the constrained equation of motions in time. The corresponding finite dimensional optimization is solved with the interior point method using the solver IPOPT [10].

This approach provides the possibility to simulate human-like motions of typical working procedures. As an application example the simulation results of the task *"lifting a box from a lower to a higher position"* are investigated, with prescribed start and end position, and the motion itself generated via optimal control.

This work is structured as follows: In section 2 the biomechanical multibody model and its dynamical equations are described. The optimal control problem and the associated solution procedure are the main topic of section 3. The simulation results of the test case of lifting a box are presented in section 4.

2. Biomechanical multibody system

In this section the underlying rigid body dynamics including the muscles as actuators are briefly presented, more details can be found in [4]. In section 2.1 the dynamics of a single rigid body is presented. The computation of the dynamics of a MBS in the special structure of a kinematic tree is outlined in section 2.2. In section 2.3 the equations of motion of such a system with additional constraints is derived. The rheological model of the muscles and their connection to the MBS are the topic of section 2.4.

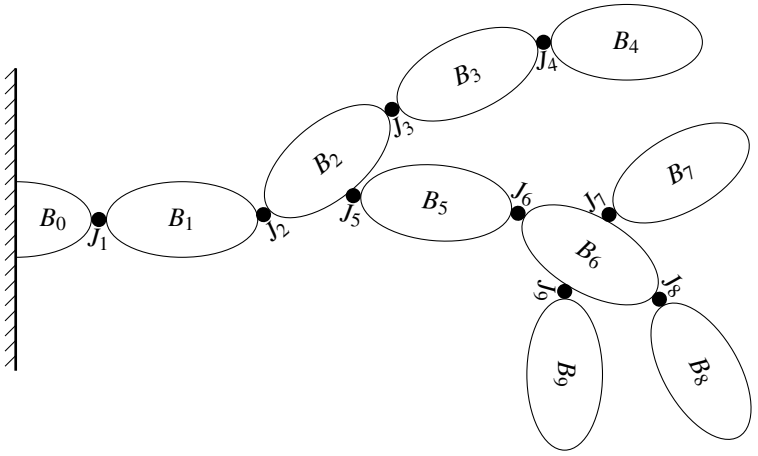

Figure 1: Example of a tree structured MBS with $N = 9$.

2.1. Rigid body

The inertial properties of a rigid body B is completely defined by a vector $\mathbf{x} \in \mathbb{R}^3$ pointing to the center of mass, its mass $m \in \mathbb{R}$ and its rotational inertia tensor $\mathsf{I} \in \mathbb{R}^3$. As in [4] spatial vector algebra is used to simplify the calculation. The velocity of the body is given by a six dimensional vector

$$\mathbf{V} = \begin{pmatrix} \boldsymbol{\omega} \\ \mathbf{v} \end{pmatrix} \in \mathbb{R}^6 \,, \tag{1}$$

where $\boldsymbol{\omega} \in \mathbb{R}^3$ is the angular velocity and $\mathbf{v} \in \mathbb{R}^3$ is the translational velocity. The spatial inertia tensor is given by

$$\mathsf{J} = \begin{pmatrix} \mathsf{I} + m\hat{\mathbf{x}}\hat{\mathbf{x}}^T & m\hat{\mathbf{x}} \\ m\hat{\mathbf{x}}^T & m\mathbb{1} \end{pmatrix} \,, \tag{2}$$

where $\hat{(\cdot)} : \mathbb{R}^3 \to \mathfrak{so}(3)$ maps a vector to a skew symmetric matrix such that $\hat{\mathbf{x}}\mathbf{y} = \mathbf{x} \times \mathbf{y}$ holds for all $\mathbf{y} \in \mathbb{R}^3$. Hence, the spatial momentum of the rigid body is given by $\mathbf{P} = \mathsf{J}\mathbf{V}$. The components of $\mathbf{P}$ are the linear and angular momentum. Combining the force $\mathbf{f} \in \mathbb{R}^3$ and the torque $\boldsymbol{\tau} \in \mathbb{R}^3$ to a spatial force $\mathbf{R} := [\boldsymbol{\tau}^T, \mathbf{f}^T]^T$ acting on the body, the Newton–Euler equations describing the motion of the rigid body are given by

$$\frac{\mathrm{d}}{\mathrm{d}t}\mathbf{P} = \mathsf{J}\frac{\mathrm{d}}{\mathrm{d}t}\mathbf{V} - \tilde{\mathbf{V}}^T\mathsf{J}\mathbf{V} = \mathbf{R} \,. \tag{3}$$

Here $\tilde{(\cdot)} : \mathbb{R}^6 \to \mathbb{R}^{6\times 6}$ maps a spatial vector to a spatial matrix according to:

$$\tilde{\mathbf{V}} = \begin{pmatrix} \tilde{\mathbf{w}} \\ \mathbf{v} \end{pmatrix} = \begin{pmatrix} \hat{\mathbf{w}} & 0 \\ \hat{\mathbf{v}} & \hat{\mathbf{w}} \end{pmatrix} \,. \tag{4}$$

2.2. Kinematic tree

A kinematic tree is a MBS system without closed loops. Such a system consists of N rigid bodies B_i, which are connected by N joints J_i. Additionally a base body B_0 is introduced which represents the resting world frame. It is assumed that joint J_i connects the body B_i with its parent $B_{p(i)}$, where the mapping $p : \mathsf{I} \to \mathsf{I}$ maps the index $i \in \mathsf{I} := \{0, 1, ..., \mathrm{N}\}$ of the body B_i to the index $p(i)$ of its parent $B_{p(i)}$. The indices of the bodies are chosen such that $p(i) < i$ holds. The vector $\mathbf{q}_i \in \mathbb{R}^{n_i}$ represent the coordinates of the joint J_i, where n_i is the number of degrees of freedom. Therefore, the configuration of the MBS is given by the vector $\mathbf{q} = [\mathbf{q}_1^T, \mathbf{q}_2^T, ..., \mathbf{q}_N^T]^T \in \mathbb{R}^n$, which implies that the whole system has $n = \sum_{i=1}^{N} n_i$ degrees of freedom. The mapping $\kappa : \mathsf{I} \to \mathscr{P}(\mathsf{I})$ delivers the ordered set of body indices, which are passed propagating backwards from B_i to base. In each joint J_i a transformation from $B_{p(i)}$ to B_i is given by

$$ {}^{i}\mathsf{X}_{p(i)} = \begin{pmatrix} \mathsf{R}_i & 0 \\ -\mathsf{R}_i \hat{\mathbf{r}}_i & \mathsf{R}_i \end{pmatrix} , \tag{5} $$

where $\mathsf{R}_i \in SO(3)$ is a rotation and $\mathbf{r}_i$ is the relative displacement, which both in general depend on the joint configuration $\mathbf{q}_i$. Because of the tree structure of the system, the spatial velocity of the body B_i can be evaluated recursively according to

$$ \mathbf{V}_i = \sum_{j \in \kappa(i)} \mathsf{S}_j(\mathbf{q}_j) \dot{\mathbf{q}}_j , \tag{6} $$

where $\mathsf{S}_j(\mathbf{q}_j) \in \mathbb{R}^{6 \times n_j}$ is the motion subspace of joint J_j. This together with the spatial inertia tensors J_i yields the following formula for the kinetic energy of the MBS

$$ T(\mathbf{q}, \dot{\mathbf{q}}) = \frac{1}{2} \sum_{i=1}^{N} \mathbf{v}_i^T \mathsf{J}_i \mathbf{v}_i = \frac{1}{2} \sum_{i=1}^{\mathrm{N}} \sum_{k \in \kappa(i)} \sum_{l \in \kappa(i)} \dot{\mathbf{q}}_k^T \mathsf{S}_k^T(\mathbf{q}_k) \mathsf{J}_i \mathsf{S}_l(\mathbf{q}_l) \dot{\mathbf{q}}_l = \dot{\mathbf{q}}^T \mathsf{M}(\mathbf{q}) \dot{\mathbf{q}} . \tag{7} $$

Hence, the kinetic energy of the system and the corresponding derivatives can be calculated by a recursion starting with the base body B_0, whereby the computational cost scales linearly with the number of rigid bodies N. There is also a fast way to compute the reduced forces acting on the rigid body with the same cost. For more details we refer to [4, 6].

2.3. Constrained mechanics

When closed loops occur in the system, as it is the case in the box lift example below, the MBS has to fulfill additional holonomic constraints $\mathbf{g} : \mathbb{R}^n \to \mathbb{R}^m$. Let $\mathbf{q} : [t_0, t_F] \to \mathbb{R}^n$ be the evolution of the MBS configuration, then the Lagrangian $L : [t_0, t_f] \to \mathbb{R}$ of the system is given by $L = T - V$, where T is the kinetic energy (7) and V is the potential energy. Additionally, a non-conservative external force $\mathbf{F}(\mathbf{q}, \dot{\mathbf{q}}, \mathbf{u}) \in \mathbb{R}^n$ is acting on the system, where $\mathbf{u} : [t_0, t_F] \to R^k$ is a external actuation. With the Lagrangian multipliers $\boldsymbol{\lambda} : [t_0, t_F] \to \mathbb{R}^m$ the Lagrange-d'Alembert principle states

$$ \delta \int L(\mathbf{q}, \dot{\mathbf{q}}) + \mathbf{g}(\mathbf{q}) \cdot \boldsymbol{\lambda} \mathrm{d}t + \int \mathbf{F}(\mathbf{q}, \dot{\mathbf{q}}, \mathbf{u}) \cdot \delta \mathbf{q} \mathrm{d}t = 0 . \tag{8} $$

By taking the variation of the first term with respect to $\mathbf{q}$ and $\boldsymbol{\lambda}$, the constrained equations of motion are given by

$$ \frac{\partial L}{\partial \mathbf{q}}(\mathbf{q}, \dot{\mathbf{q}}) - \frac{\mathrm{d}}{\mathrm{d}t} \frac{\partial L}{\partial \dot{\mathbf{q}}}(\mathbf{q}, \dot{\mathbf{q}}) + \mathbf{F}(\mathbf{q}, \dot{\mathbf{q}}, \mathbf{u}) + \mathsf{G}^T(\mathbf{q}) \boldsymbol{\lambda} = 0 , \tag{9} $$

$$ \mathbf{g}(\mathbf{q}) = 0 , \tag{10} $$

where $\mathsf{G} : \mathbb{R}^n \to \mathbb{R}^{m \times n}$ denotes the derivative $\mathsf{G} = \frac{\partial \mathbf{g}}{\partial \mathbf{q}}$ of the constraint function with respect to the configuration.

2.4. Muscles

To actuate the multibody model representing the human skeleton, a simplified mathematical muscle model of Hill type is used, as in [1, 3]. The rheological model of the muscle consists of a contractile element (CC) and an elastic spring (PE), as sketched in the left image of Figure 2. The force generated by the CC depends on the current length l, the contraction velocity $\dot{l}$, the actuation level $u \in [0, 1]$ and the maximal isometric force $F_{\max}$ of the muscle and is given by $F_{CC} = f_l(l) f_v(\dot{l}) u F_{\max}$. The length and the velocity dependencies are approximated by the following two functions

$$ f_l(l) = 1 - \frac{(l - l_{\mathrm{opt}})^2}{(l_{\mathrm{opt}} - l_0)^2} \qquad f_v(v) = \begin{cases} \frac{v_{\max} - v}{v_{\max} + \frac{v}{\gamma}} & v \geq 0 \\ \frac{A}{\frac{v}{v_{\max}} - B} + C & v < 0 \end{cases} . \tag{11} $$

Here l_0 represents the minimal and l_{opt} the optimal muscle length. The negative scalar $v_{\max} < 0$ is the maximal contractive velocity of the muscle, and γ is a shape factor, while $A, B, C \in \mathbb{R}$ are chosen such that the function is differentiable in 0. Both functions are visualized in Figure 3.

The PE element is approximated by a linear elastic spring $F_{PE} = k(l - l_0)$ with stiffness $k \in \mathbb{R}_+$. Since the elements are connected in parallel, the muscle force is a linear superposition of both

$$F_m = F_{CC} + F_{PE} = k(l - l_0) + f_l(l) f_v(v) u F_{\max} \,. \tag{12}$$

To use the rheological Hill elements in MBS a piecewise linear string is used as approximation of the muscle path. This string is defined by at least two points x_I,where each is rigidly connected to a rigid body $B_{i(I)}$. The length of the muscle is calculated by summarizing the distance between the points expressed in the base coordinate system $l = \sum \|x_I - x_{I-1}\|$, while the velocity is calculated equivalently. With these quantities and an actuation u, the scalar muscle force $F_m \in \mathbb{R}$ is calculated by (12). Then in every point x_i a force pointing into the direction straight direction to the neighboring points with magnitude F_m is applied, which induces a force and a torque in the corresponding body. In the right image of Figure 2 two string muscles are visualized. It has to be noted that in this scenario the muscle is only allowed to create pulling forces like in reality.

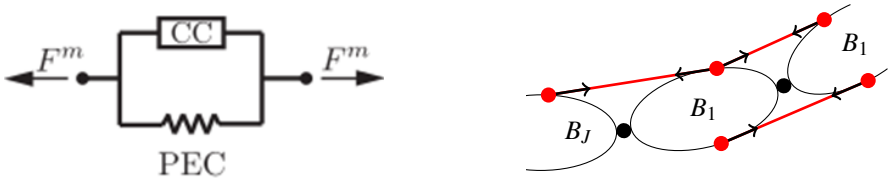

Figure 2: **Left:** Simplified Hill muscle model. **Right:** MBS with Hill-muscle strings and corresponding forces.

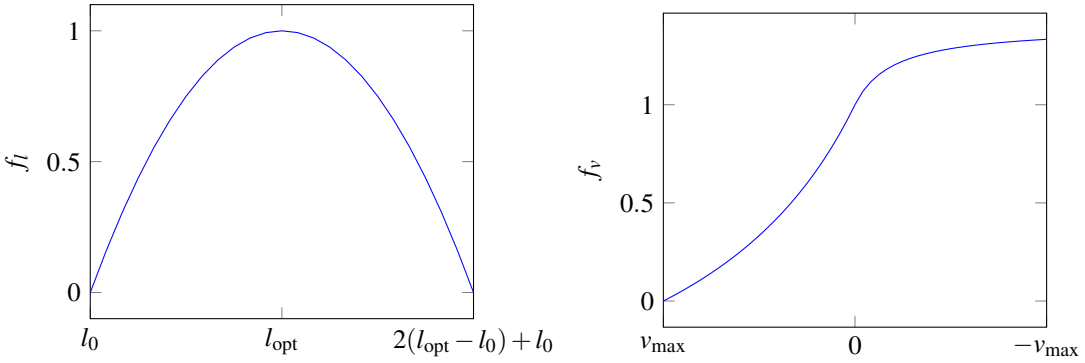

Figure 3: **Left:** Length dependency of CC-element. **Right:** Velocity dependency of CC-elements, where v>0 corresponds to a eccentric and v<0 to a concentric motion.

3. Optimal Control

Optimal control is a special class of infinite optimization problems on functions spaces, see [11]. Optimal control problems for the biomechanical MBS treated in this work may be formulated as follows:

$$\text{Minimize } J = \int_{t_0}^{t_F} \phi\left(\mathbf{q}, \dot{\mathbf{q}}, \mathbf{u}\right) \mathrm{d}t + \chi\left(\mathbf{q}|_{t_0}, \mathbf{q}|_{t_F}, t_0, t_F\right) \tag{13}$$

$$\frac{\partial L}{\partial \mathbf{q}}(\mathbf{q}, \dot{\mathbf{q}}) - \frac{\mathrm{d}}{\mathrm{d}t}\frac{\partial L}{\partial \dot{\mathbf{q}}}(\mathbf{q}, \dot{\mathbf{q}}) + \mathbf{F}(\mathbf{q}, \dot{\mathbf{q}}, \mathbf{u}) + \mathsf{G}^T(\mathbf{q})\boldsymbol{\lambda} = 0 \,, \tag{14}$$

$$\mathbf{g}(\mathbf{q}) = 0 \,, \tag{15}$$

$$\mathbf{c}^- \leq \mathbf{c}(\mathbf{q}, \mathbf{u}, \boldsymbol{\lambda}) \leq \mathbf{c}^+ \,. \tag{16}$$

As already introduced in section 2, the functions $\mathbf{q} : [t_0, t_F] \to \mathbb{R}^n$, $\mathbf{u} : [t_0, t_F] \to \mathbb{R}^k$ and $\boldsymbol{\lambda} : [t_0, t_F] \to \mathbb{R}^m$ represent the evolution of the configuration of the MBS, the control and the Lagrangian multiplier in the time interval $[t_0, t_F]$. The

main goal of minimizing the objective function J is introduced in (13). As a side constraint the constrained equations of motion (14)-(15) have to be fulfilled by the mappings $\mathbf{q}, \mathbf{u}$ and $\boldsymbol{\lambda}$. Additional equality and inequality constraints are included to the optimal control problem by (16). It has to be noted that it is also possible to include the start t_0 and end time t_F as unknown variables, see [11].

In this section the solution strategy for (13)-(16) is outlined. In section 3.1 five different objective functions are introduced, which will be used later on in this work, section 3.2 explains the DMOCC approach as a solution procedure for the optimal control problem, and a strategy to include contact between rigid bodies into the optimal control framework is presented in section 3.3.

3.1. Objective functions

The main scope of the approach presented in this work is to create human like motion for specific tasks modeled with help of optimal control. Therefore the following five objective functions

$$J_u = \int_{t_0}^{t_F} \mathbf{u} \cdot \mathbf{u} \, \mathrm{d}t \;, \quad J_{\dot{u}} = \int_{t_0}^{t_F} \dot{\mathbf{u}} \cdot \dot{\mathbf{u}} \, \mathrm{d}t \;, \quad J_T = \int_{t_0}^{t_F} T \, \mathrm{d}t \;, \quad J_t = t_f \;, \quad J_{\mathrm{mix}} = c_u J_u + c_{\dot{u}} J_{\dot{u}} + c_T J_T + c_t J_t \;, \tag{17}$$

are investigated, where J_u is minimal control, $J_{\dot{u}}$ is minimal control change, J_T minimal kinetic energy and J_t minimal duration. The last objective function J_{mix} is a linear combination of the other ones, with parameters c_u, $c_{\dot{u}}$, c_T and c_t adjusted such that the solution of the optimal control problem corresponds to a human-like motion with realistic muscle actuation. Therefore the four other objective functions have been investigated, and the characteristics of the corresponding motions have been used to choose a proper linear combination.

3.2. DMOCC

To solve (13)-(16) the so called DMOCC method from [9] is applied, which belongs to the class of direct transcription methods, where the optimal control problem is discretized in time, and the resulting finite dimensional optimization problem is then solved. In the DMOCC approach, additionally a variational integration is used for the constrained equations of motion (14)-(15). Therefore, the discretization is already applied in (8), and the variation is applied to the discrete equations.

The evolution of the configuration $\mathbf{q}$, the control signal $\mathbf{u}$ and the Lagrangian multipliers $\boldsymbol{\lambda}$ are discrtized by $N+1$ samples $\mathbf{q}^I \in \mathbb{R}^n$, $\mathbf{u}^I \in \mathbb{R}^k$ and $\boldsymbol{\lambda}^I \in \mathbb{R}^m$ with a fixed time step size $h := \frac{t_F - t_0}{N}$, i.e. $\mathbf{q}^I$ is an approximation of the continuous function $\mathbf{q}$ at $t_I := t_0 + hI$. On this basis a discrete Lagrangian L_d is constructed with the following approximation

$$L_d\left(\mathbf{q}^I, \mathbf{q}^{I+1}\right) \approx \int_{t_I}^{t_{I+1}} L(\mathbf{q}, \dot{\mathbf{q}}) \mathrm{d}t \;. \tag{18}$$

Additionally the action integral over the non conservative force is approximated by

$$F_g^-(\mathbf{q}^I, \mathbf{q}^{I+1}, \mathbf{u}^I, \mathbf{u}^{I+1}) \cdot \delta\mathbf{q}^I + F_g^+(\mathbf{q}^I, \mathbf{q}^{I+1}, \mathbf{u}^I, \mathbf{u}^{I+1}) \cdot \delta\mathbf{q}^{I+1} \approx \int_{t_I}^{t_{I+1}} \mathbf{F}(\mathbf{q}, \dot{\mathbf{q}}, \mathbf{u}) \cdot \delta\mathbf{q} \mathrm{d}t \;, \tag{19}$$

where $\delta\mathbf{q}^I$ is the discrete variation in t_I. The integral over the scalar product of the constraint equation and the Lagrangian multiplier is discretized by

$$\frac{h}{2}\left(\mathbf{g}(\mathbf{q}^I) \cdot \boldsymbol{\lambda}^I + \mathbf{g}(\mathbf{q}^{I+1}) \cdot \boldsymbol{\lambda}^{I+1}\right) \approx \int_{t_I}^{t_{I+1}} \mathbf{g}(q) \cdot \boldsymbol{\lambda} \mathrm{d}t \;. \tag{20}$$

Altogether, the variation of the discrete version of (8) with respect to $\mathbf{q}^I$ and $\boldsymbol{\lambda}^I$ reads

$$\begin{aligned} \sum_{I=0}^{N-1} \Bigg[& \left(\partial_1 L_d(\mathbf{q}^I, \mathbf{q}^{I+1}) + \frac{h}{2} G(\mathbf{q}^I) \boldsymbol{\lambda}^I + F_-^h(\mathbf{q}^I, \mathbf{q}^{I+1}, \mathbf{u}^I, \mathbf{u}^{I+1})\right) \cdot \delta\mathbf{q}^I \\ & + \left(\partial_2 L_d(\mathbf{q}^I, \mathbf{q}^{I+1}) + \frac{h}{2} G(\mathbf{q}^{I+1}) \boldsymbol{\lambda}^{I+1} + F_+^h(\mathbf{q}^I, \mathbf{q}^{I+1}, \mathbf{u}^I, \mathbf{u}^{I+1})\right) \cdot \delta\mathbf{q}^{I+1} + \frac{h}{2} \mathbf{g}(\mathbf{q}^I) \cdot \delta\boldsymbol{\lambda}^I + \frac{h}{2} \mathbf{g}(\mathbf{q}^I) \cdot \delta\boldsymbol{\lambda}^I \Bigg] = 0 \;, \end{aligned} \tag{21}$$

where $\partial_\alpha L_d$ is the partial derivative of the discrete Lagrangian with respect to the first respectively the second input $\alpha \in 1, 2$. Additionally to (21) initial conditions for $\mathbf{q}_0$, $\dot{\mathbf{q}}_0$, $\mathbf{q}_N$ and $\dot{\mathbf{q}}_N$ can be included (see [8] for further details).

Finally, the integral of the objective function (13) is approximated by $\phi_d(\mathbf{q}^I,\mathbf{q}^{I+1},\mathbf{u}^I,\mathbf{u}^{I+1}) \approx \int_{t_I}^{t_{I+1}} \phi(\mathbf{q},\dot{\mathbf{q}},\mathbf{u})\mathrm{d}t$. Hence, the discrete version of the optimal control problem (13)-(16) is given by

$$\text{Minimize } J^h = \sum_{I=0}^{N-1} \phi_d(\mathbf{q}^I,\mathbf{q}^{I+1},\mathbf{u}^I,\mathbf{u}^{I+1}) + \chi(\mathbf{q}^0,\mathbf{q}^N,t_0,t_N) \tag{22}$$

$$\partial_2 L_d(\mathbf{q}_{I-1},\mathbf{q}_I) + \partial_1 L_d(\mathbf{q}_I,\mathbf{q}_{I+1}) + \mathbf{F}_-^h(\mathbf{q}_I,\mathbf{q}_{I+1},\mathbf{u}_I) + \mathbf{F}_+^h(\mathbf{q}_{I-1},\mathbf{q}_I,\mathbf{u}_{I-1}) + G^T(\mathbf{q}_I)\boldsymbol{\lambda}_I = 0 \qquad I = 1,...,N-1 \tag{23}$$

$$\mathbf{g}(\mathbf{q}_I) = 0 \qquad I = 0,...,N \tag{24}$$

$$\mathbf{c}_-^h \le \mathbf{c}^h(\mathbf{q}^I,\mathbf{u}^J,\boldsymbol{\lambda}^K) \le \mathbf{c}_+^h\,, \tag{25}$$

where (25) is a proper discretization of (16). The equations (22)-(25) define a finite dimensional nonlinear optimization problem, which is solved with an interior point method implemented in the solver IPOPT [10].

3.2.1. Trapezoidal rule

In the results of this work a trapezoidal rule is used to approximate the integrals, which yields

$$L_d(\mathbf{q}^I,\mathbf{q}^J) = \frac{h}{2}L\left(\mathbf{q}^I,\frac{\mathbf{q}^J-\mathbf{q}^I}{h}\right) + \frac{h}{2}L\left(\mathbf{q}^J,\frac{\mathbf{q}^J-\mathbf{q}^I}{h}\right)\,, \tag{26}$$

$$\mathbf{F}_d^-(\mathbf{q}^I,\mathbf{q}^J,\mathbf{u}^I,\mathbf{u}^J) = \frac{h}{2}\mathbf{F}\left(\mathbf{q}^I,\frac{\mathbf{q}^J-\mathbf{q}^I}{h},\mathbf{u}^I\right)\,, \qquad \mathbf{F}_d^+(\mathbf{q}^I,\mathbf{q}^J,\mathbf{u}^I,\mathbf{u}^J) = \frac{h}{2}\mathbf{F}\left(\mathbf{q}^J,\frac{\mathbf{q}^J-\mathbf{q}^I}{h},\mathbf{u}^J\right)\,, \tag{27}$$

$$\phi_d(\mathbf{q}^I,\mathbf{q}^J,\mathbf{u}^I,\mathbf{u}^J) = \frac{h}{2}\phi\left(\mathbf{q}^I,\frac{\mathbf{q}^J-\mathbf{q}^I}{h},\mathbf{u}^I\right) + \frac{h}{2}\phi\left(\mathbf{q}^J,\frac{\mathbf{q}^J-\mathbf{q}^I}{h},\mathbf{u}^J\right)\,. \tag{28}$$

$$\tag{29}$$

The corresponding derivatives ∂L_d can be computed by exploiting the chain rule.

3.3. Contact

In this work, contact between two rigid bodies is restricted to a constraint, which rigidly connects both bodies. Hence, there is no relative translation and rotation between the bodies if the constraint is satisfied. The presented concept could be easily enhanced to other contact scenarios. A similar methodologyy to include arbitrary contact points in optimal control can be found in [13, 14].

In this section, several enhancements are introduced to include contact into the optimal control problem. First, a method to switch the contact constraint on and off and to compute the corresponding force using multiple phases is presented. Additionally, a concept is outlined how an arbitrary contact point could be included into the optimal control problem. Finally, an approach is shown how the contact constraint forces could be restricted to frictional sticking contact.

3.3.1. Concept of phases

To include contact between rigid bodies into the optimal control approach multiple phases are used, where different additional constraints are applied. Therefore the interval $\mathtt{I} = [t_0,t_F]$ is divided into a finite number $M \in \mathbb{N}$ of distinct sub-intervals $\mathtt{I}_i := [t_{0_I},t_{F_I}]$, which fulfill

$$t_{F_I} = t_{0_{I+1}} \qquad \text{for} \qquad I = 1,..,M-1\,. \tag{30}$$

The constrained equations of motion on each interval are given by (14)-(15), containing an extra constraint $\mathbf{g}_I : \mathbb{R}^N \to \mathbb{R}^{M_I}$ with corresponding Lagrangian multiplier $\boldsymbol{\lambda}_I : \mathtt{I}_I \to \mathbb{R}^{M_I}$. Hence, in every phase $\mathtt{I}_I$ the DAE system

$$\frac{\partial L}{\partial \mathbf{q}}(\mathbf{q},\dot{\mathbf{q}}) - \frac{\mathrm{d}}{\mathrm{d}t}\frac{\partial L}{\partial \dot{\mathbf{q}}}(\mathbf{q},\dot{\mathbf{q}}) + \mathbf{F}(\mathbf{q},\dot{\mathbf{q}},\mathbf{u}) + \mathsf{G}^T(\mathbf{q})\boldsymbol{\lambda} + \mathsf{G}_I^T(\mathbf{q})\boldsymbol{\lambda}_I = 0\,, \tag{31}$$

$$\mathbf{g}(\mathbf{q}) = 0\,, \tag{32}$$

$$\mathbf{g}_I(\mathbf{q}) = 0 \tag{33}$$

has to be fulfilled, where again $(G)_I$ denotes the derivative of $\mathbf{g}_I$ with respect to $\mathbf{q}$. This model provides the possibility to switch on and off the contact condition between two phases. Because the start and end time of each phase are also

unknowns, restricted by (30) only, the time point when the contact closes or opens is part of the solution of the optimal control problem. This method may be incorporated into the DMOCC approach in a straightforward manner by applying the respective variational integrator to each phase. Note that at the transition between phases it could be necessary to add the velocity constraint

$$\mathsf{G}_I^T(\mathbf{q})\dot{\mathbf{q}} = 0\,, \tag{34}$$

at the beginning t_{0_I} or the end t_{F_I} of a phase to prevent the constraint forces from adding work to the system.

3.3.2. Arbitrary contact point

To enable the contact point itself to be arbitrary, a master-slave concept used. Therefore, in the slave body the contact point is assumed to be given by $\mathbf{x}_s \in \mathbb{R}^3$. The contact point on the master body $\mathbf{p}_\mathbf{x} \in \mathbb{R}^3$ is added as a parameter to the optimal control problem (13)-(16). In a rigid connection also the relative rotation between two bodies is prescribed, therefore an additional parameter $\mathbf{p}_\mathsf{R}$ parametrizing the transformation matrix $\mathsf{R}(\mathbf{p}_\mathsf{R})$ from the master to the slave body is introduced. Let $\mathsf{R}_s \in SO(3)$ be the rotation and $\mathbf{r}_s \in \mathbb{R}^3$ the translation from base to the slave body. Then the same transformations given by R_m and $\mathbf{r}_m$ apply to the master body, resulting in the rigid contact constraint

$$\mathbf{g}_c = \begin{pmatrix} \mathsf{R}_m\mathsf{R}_s^T\mathbf{x}_s - \mathbf{p}_\mathbf{x} \\ \log\left(\mathsf{R}^T(\mathbf{p}_\mathsf{R})\mathsf{R}_m\mathsf{R}_s^T\right) \end{pmatrix}\,, \tag{35}$$

where $\log : SO(3) \to \mathfrak{so}(3) \simeq \mathbb{R}^3$ denotes the inverse of the Rodriguez-formula, including the usual identification of skew-symmetric matrices and vectors.

3.3.3. Sticking contact

By including additional unknown parameters into the optimal control problem one may also include frictional sticking contact between two bodies. The two bodies B_s and B_m with corresponding transformations $(\mathbf{r}_s, \mathsf{R}_s)$ and $(\mathbf{r}_m, \mathsf{R}_m)$ are rigidly connected, by a constraint equation $\mathbf{g}_c(\mathbf{q})$. It is assumed that the corresponding constraint force $\mathsf{G}_c^T(\mathbf{q})\boldsymbol{\lambda}$ can be decomposed into a global force $\mathbf{f}_c \in \mathbb{R}^3$ and a torque $\boldsymbol{\tau}_c \in \mathbb{R}^3$. In the slave body a finite number $K \in \mathbb{N}$ of fixed positions $\mathbf{x}_{s_i}$ representing virtual contact points are defined. For each of these a parameter $\mathbf{p}_i \in \mathbb{R}^3$ is added to every time point in the optimal control problem[1]. As these parameters should represent the local contact force, the constraints

$$\mathbf{f}_c = \sum_{i=1}^{K} \mathbf{p}_i \qquad \text{and} \qquad \boldsymbol{\tau}_c = \sum_{i=1}^{K} (\mathbf{r}_s + \mathsf{R}_s^T\mathbf{x}_{s_i}) \times \mathbf{p}_i \tag{36}$$

have to be fulfilled, such that the parameters $\mathbf{p}_i$ yield a possible distribution of the constraint forces. In sticking contact the tangential force $\mathbf{f}_\mathbf{T}$ is restricted by the normal pressure $p_\mathbf{N} > 0$, and the frictional constant $\mu \in \mathbb{R}$ by the inequality $\|\mathbf{f}_\mathbf{T}\| \leq \mu p_\mathbf{N}$. To transfer this to the local forces $\mathbf{p}_i$, a normal vector $\mathbf{N}_m$ in the master body is defined. Therefore the sticking contact constraint in a contact point $\mathbf{x}_{s_i}$ reads

$$\| \mathbf{p}_i - (\mathbf{p}_i \cdot R_m^T\mathbf{N}_m)R_m^T\mathbf{N}_m\| \leq \mu\mathbf{p}_i \cdot R_m^T\mathbf{N}_m\,. \tag{37}$$

By adding the equations (36) and (37) as constraints to the optimal control problem, the constraint force $\mathsf{G}_c^T(\mathbf{q})\boldsymbol{\lambda}$ is implicitly restricted to frictional sticking contact with respect to contact points $\mathbf{x}_{s_i}$ and the normal $\mathbf{N}_m$.

4. Box lift simulation

As application case we consider lifting of a box by two arms from a lower to a higher position. Each arm consists of four bodies, upper arm, ulna, radius and hand, which are serially connected by four links, where the shoulder is modeled as a spherical joint, the elbow is split into two revolute joints and the wrist is represented by a universal joint. The box is allowed to freely translate and rotate with respect to the base frame, which corresponds to a six-dimensional joint. To actuate the MBS each arm is equipped with 29 Hill-muscle strings, as described in section 2.4. Altogether there are 20 degrees of freedom $\mathbf{q} \in \mathbb{R}^{20}$ controlled by 58 control signals $\mathbf{u} \in \mathbb{R}^{58}$. To include the process of grabbing the box, the equations of motion are split into two phases, as discussed in section 3.3.1. In the first phase the box is rigidly connected to a fixed frame by a corresponding constraint force, where at the end of the phase the hidden

[1] In the continuous case this would lead to an additional function $\mathbf{p}_i : \mathtt{I} \to \mathbb{R}^3$, while in the discrete scenario in every node time t_I $I = 0,..,N$ an additional parameter is added.

constraint (34) has to be added to the optimal control problem. The start position for both arms is prescribed by given joint angles, see left pictures in Figure 4. In the second phase both hands are rigidly connected to each side of the box, while the corresponding contact point on each side of the box is unknown, see section 3.3.2. Again the associated hidden constraint (34) has to be added at the start of this phase. To ensure frictional sticking with $\mu = 1$ between the hands and the box, at each hand four contact nodes are defined in the corners of the cuboid and in each contact side of the box a contact normal is defined, see section 3.3.3. Therefore, both arms have to press the box against each others to be able to lift it. At the end of the second phase the box should be positioned such that it matches a prescribed frame. The start point of the first phase is fixed to zero, such that the unknown end time t_F of phase two gives the duration of the whole motion, which is bound from above by the maximum execution time of two seconds.

In Figure 4 the motions generated by the different objective function from (17) are shown as image sequence. The

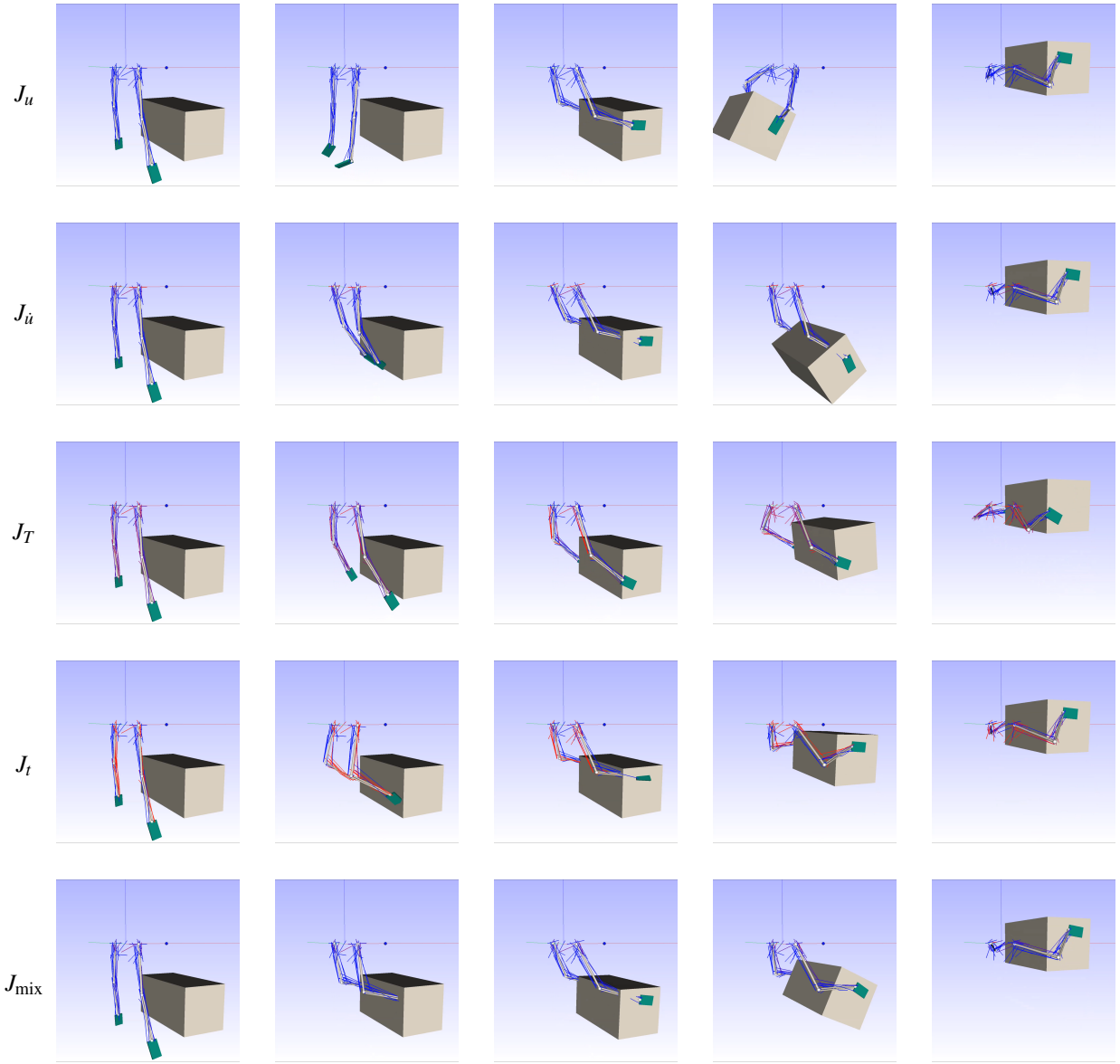

Figure 4: Image sequence of the use case box lift, where each row represents a different objective functions and each column a discrete time node.

color of the string muscles induce the actuation level, where blue represents zero and red full activation. In the case of minimal actuation J_u it could be noticed that the system tries to use as much inertia as possible. Therefore, the box and the arms perform a swing motion to reach the final position. The robot like motions generated by minimizing the control change $J_{\dot{u}}$ can hardly be depicted in the image sequence. By minimizing the kinetic energy the system tries to move minimally and as slow as possible, which can be seen by the narrow grabbing position, which inevitably induces a

lot of work for the muscles (as indicated by the color of the muscles). In the case of minimal execution time, the motion looks naturally, but most of the muscles are fully actuated, which certainly would yield to an unfavorable ergonomic assessment of the work task. The parameter values used for the simulation for this test case are $c_u = 0.1$, $c_{\dot{u}} = 0.01$, $c_T = 0.1$ and $c_t = 1$. Finally the mixed objective function J_{mix} yields a realistic human like motion as desired, with muscle actuations not exploited to their maximum possible values.

In Figure 5 the actuation signal of the anterior deltoid is plotted against time for all objective functions. This muscle

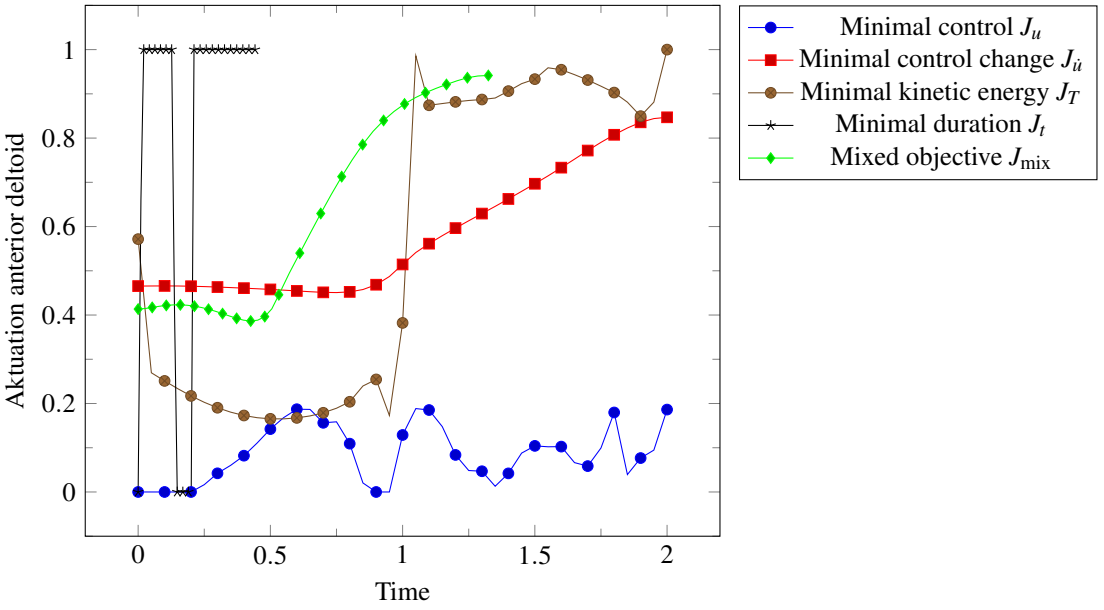

Figure 5: Control signal of the anterior deltoid muscle for the five different control signals.

is chosen as a representative, because it is one of the main actors when performing frontal lifting. At first one notices that the signals differ in length because of the different execution times. The signal generated by J_u has the lowest amplitude as expected due to the generated swingin motion that exploits inertia, and the characteristics of the actuation likewise differs from those of the other signals. By minimizing the control change, a nearly constant signal is achieved for the first phase, while in the second phase, where the box is connected to the hands, the actuation is almost linearly increasing. The minimization of the kinetic energy J_T yields a jump in the control signal at the transition between the two phases, which compensates the sudden loss of the constraint force holding the box. The shortest signal is of course generated by minimizing the duration, which is achieved by either maximum or zero actuation. This is holds likewise for all other muscle actuation signals (not displayed here, as they have the same characteristics). The signal generated by the mixed objective function results in a smooth motion of realistic duration. When the arms are moved to the box in the first phase, the signal is constant due to the constant moderate flexion of the shoulder, as can be seen in the last row of Figure 4. In the second phase, where the box is lifted due to the flexion of the shoulder, the signal is increasing.

5. Conclusion and further work

In this work a method to create human like motion for the simulation of working tasks has been presented. As application case two arms equipped with muscles as actuators lifting a box with frictional contact has been investigated. In further work the results from simulation will be validated against EMG-measurements and motion capture data.

Acknowledgments

This work was supported by the Fraunhofer Internal Programs under Grant No. MAVO 828 424.

References

[1] R. Maas and S. Leyendecker. Optimal control of biomechanical motion using physiologically motivated cost functions. The 2nd joint international conference on multibody system dynamics, 2012.

[2] R. Mass and S Leyendecker. "Muscle paths in biomechanical multibody simulations." Proceedings of ECCOMAS Multibody Dynamics Conference, Zagreb, Croatia. 2013.

[3] R. Maas and S. Leyendecker. Biomechanical optimal control of human arm motion. Proceedings of the Institution of Mechanical Engineers, Part K: Journal of Multi-body Dynamics, 2013.,

[4] R. Featherstone. Rigid body dynamics algorithm. Springer, 2014.

[5] S. Björkenstam, N. Delfs, J. S. Carlson, R. Bohlin and B. Lennartson. Enhancing digital human motion planning of assembly tasks through dynamics and optimal control. Procedia CIRP, 44, 20-25. , 2016.

[6] S. Björkenstam, S. Leyendecker, J. S. Carlson, and B. Lennartson. Inverse dynamics for discrete mechanics of multibody systems with application to direct optimal control. Submitted for publication, 2016.

[7] F. E. Zajac. Muscle and tendon: properties, models, scaling, and application to biomechanics and motor control. Critical reviews in biomedical engineering, 17(4), 359-411, 1989.

[8] J. Marsden and M. West. Discrete mechanics and variational integrators. Acta Numerica,10 , 957-514, 2001.

[9] S. Leyendecker, S. Ober-Blöbaum, J. Marsden and M. Ortiz. Discrete mechanics and optimal control for constrained systems. Optimal control applications & methods, 31(6), 505–528, 2010.

[10] A. Wächter and L. T. Biegle. On the Implementation of a Primal-Dual Interior Point Filter Line Search Algorithm for Large-Scale Nonlinear Programming, Mathematical Programming 106(1), pp. 25-57, 2006.

[11] M. Gerdts. Optimal control of odes and daes. De Gruyter , 2012.

[12] J. T. Betts. Survey of numerical methods for trajectory optimization. Journal of guidance, control, and dynamics, 21(2), 193-207, 1998.

[13] M. Koch, and S. Leyendecker. Structure preserving simulation of monopedal jumping. Archive of Mechanical Engineering, 60, 127-146, 2013.

[14] M. Koch, and S. Leyendecker. Structure preserving optimal control of a three-dimensional upright gait. Multibody Dynamics: Computational Methods and Application 42, 115-146, 2016.